



Fluoride Removal from Water by Using Green Magnetic Activated Carbon Derived from Canola Stalks

George Z. Kyzas · Athanasia K. Tolkou ·
Tariq J. Al Musawi · Nezamaddin Mengelizadeh ·
Samaneh Mohebi · Davoud Balarak

Received: 25 March 2022 / Accepted: 10 October 2022 / Published online: 14 October 2022
© The Author(s), under exclusive licence to Springer Nature Switzerland AG 2022

Abstract The aim of this study was to synthesize activated carbon from canola stalks and then magnetize it with Fe_3O_4 (ACCS- Fe_3O_4) nanoparticles and evaluate it to remove fluoride (F^-) from water. First, the used adsorbent was analyzed and characterized using advanced techniques. Then, the influence of important parameters as the pH, initial fluoride concentration, adsorbent's dose, contact time, and temperature was investigated. The adsorption isotherms of Langmuir, Freundlich, Temkin, and Dubinin-Radushkevich (D-R) were analyzed in both linear and nonlinear forms using four error coefficients (SSE, HYDRID, X^2 , and MSPD). Langmuir isotherm was found to be the best-fitted model in both linear and nonlinear forms due to its high regression coefficient and lower error coefficient. The

results showed that the removal efficiency increased with increasing contact time, adsorbent's dose, and temperature, but decreased with increasing fluoride concentration and pH. Adsorbent recovery and reuse were studied and the results showed that only 8% reduction in efficiency was observed after six sequential cycles, which indicates the high performance of the adsorbent after recovery. It was also found that the adsorption of fluoride ions on ACCS- Fe_3O_4 was endothermic ($\Delta H^0 = 69.38$ kJ/mol) and spontaneous ($\Delta G^0 = -2.78$ – 10.31 kJ/mol) process. The adsorption process was better described by fitting to the pseudo-second order kinetic model (PSO). Fluoride adsorption is controlled by all three models of bulk diffusion, film diffusion, and pore diffusion.

Supplementary Information The online version contains supplementary material available at <https://doi.org/10.1007/s11270-022-05900-6>.

G. Z. Kyzas · A. K. Tolkou
Department of Chemistry, International Hellenic
University, Kavala, Greece
e-mail: kyzas@chem.ihu.gr

A. K. Tolkou
e-mail: tolkatha@chem.ihu.gr

T. J. Al Musawi
Department of Chemical Engineering and Petroleum
Industries, Al-Mustaqbal University, College, Babylon,
Iraq
e-mail: dbchemistry2@gmail.com

N. Mengelizadeh
Department of Environmental Health Engineering,
Evas Faculty of Health, Larestan University of Medical
Sciences, Larestan, Iran
e-mail: hosseinazarpira30@gmail.com

S. Mohebi
Student Research Committee, Zahedan University
of Medical Sciences, Zahedan, Iran
e-mail: youse.mahdavi@gmail.com

D. Balarak (✉)
Department of Environmental Health, Health Promotion
Research Center, University of Medical Sciences,
Zahedan, Iran
e-mail: dbalarak2@gmail.com

Keywords ACCS- Fe_3O_4 · Error coefficients · Fluoride · Adsorption equilibrium

1 Introduction

In recent years, the rapid development in industry and agriculture and the increase in population density have exacerbated the problem of environmental pollution, as studies indicate the discharge of large quantities of toxic pollutants into drinking water sources without efficient treatment, causing serious pollution that threatens human and aquatic life (Rahmani et al., 2010; Zazouli et al., 2014a, 2014b). In this regard, fluorine contamination is one of the important issues that must be addressed. Fluoride is a natural element among minerals, geochemical sediments, and natural water systems that enters the food chain through drinking water or plant nutrition (Mohammadi et al., 2017). Fluoride ion is known as the most electronegative ion, so it tends to combine with various cations such as sodium, potassium, aluminum, and zinc, and therefore is never found freely in the environment. In cases where the amount is low in water, it should be added artificially to the water (Wang et al., 2022; Premathilaka & Liyanagedera, 2019). The presence of fluoride in water is necessary to prevent tooth decay, but if the amount is too high, it can cause dental fluorosis and skeletal fluorosis (Somak & Sirshendu, 2014). Fluorosis causes weakening of the structure of the teeth and skeleton, causes growth to stagnate, and, in more severe cases, results in paralysis and death (Bharali et al., 2015; Zhen et al., 2016).

Numerous studies in recent years have shown that the long-term effects of exposure to fluoride and its accumulation not only pose skeletal and dental hazards to humans, but can also alter DNA structure (Bhau-mik et al., 2012). The World Health Organization has declared the permissible level of fluoride in water 0.75–1.5 mg/L (WHO, 2006). Due to the toxicity of fluoride and the risk of overdose, fluoridation of drinking water has stopped in some countries. Excessive concentrations of fluoride in groundwater in more than 20 developed countries, including Iran, have been reported in the research of some researchers (Bazrafshan et al., 2016; Choi et al., 2022). Other effects of exposure to excess fluoride through drinking water include staining of the teeth, damage to the endocrine glands, thyroid, liver, softening of the bones, healing of tendons and ligaments,

and a reduction in the space between the vertebrae (Bal-arak et al., 2016; Wang et al., 2020). These effects are exacerbated especially in tropical areas where people consume large amounts of water and the fluoride concentration increases due to evaporation (Kumar et al., 2011).

Fluoride contamination of water sources has two main sources, i.e., natural origin and anthropogenic origin (human industrial activities) (Tor, 2006). Fluoride is abundant in minerals and can enter water sources through water erosion and contaminate resources, especially groundwater (Jadhav et al., 2015). Also, with human progress and increasing industrial activities, more fluoride enters the environment. Industries such as aluminum and steel production, plating, metal processing, glassmaking and semiconductor production, and chemical fertilizers by using fluoride-containing compounds cause fluoride to enter the environment through wastewater disposal (Joshi et al., 2022; Borgohain and Rashid, 2022).

The presence of high concentrations of fluoride in drinking water sources in countries such as India, China, the USA, Africa, and Iran have caused many problems, so the defluoridation process is necessary in places where high concentrations of fluoride are present (Chen et al., 2010). Due to the adverse health effects of excess fluoride in the water, especially in groundwater and due to the fact that most cities in Iran use groundwater, it is necessary to take measures to eliminate the excessive fluoride (Balarak et al., 2017; Srivastav et al., 2013).

So far, various methods for fluoridation and removal of fluoride from aqueous media, including chemical precipitation, ion exchange, adsorption, electrolysis, and nanofiltration, have been studied (Bhan et al., 2022; Yu et al., 2022). In addition, various types of coagulants such as alum, ferric sulfate, ferrous sulfate, ferric chloride, anionic, cationic, and non-ionic organic polymers are used to remove organic and inorganic contaminants (Haghighat et al., 2012). Ion exchange processes and membrane processes have a high efficiency in fluoride removal and can bring the fluoride concentration to the allowable level, but since these processes are expensive and complex, they cannot be used in deprived areas (Mahvi & Mostafapour, 2019a, 2019b). Coagulation, alternatively, is a cost-effective technology for defluoridation but requires high doses and therefore produces substantial amounts of sludge.

Among the mentioned processes, the adsorption process is a cost-effective, simple, and practical

process in deprived areas (Zazouli et al., 2015). One of the most important adsorbents in the field of removal of pollutants is activated carbon that has important properties such as high adsorption and porosity, which increases the efficiency of the adsorbent, but there are two limitations in the use of activated carbon (Li et al., 2010). The first limitation is the high price of commercial carbon that limits its use, and the second limitation is related to the small size of carbon nanoparticles, which makes it difficult to collect, in other words, it is a disposable adsorbent (Yu et al., 2013).

Thus, to solve the problem, researchers are looking to produce activated carbon from inexpensive materials. Due to the abundance of agricultural waste, it is one of the cheap materials that can be troublesome at no cost and one of the environmental problems caused by the collection and burial of agricultural waste will also be solved (Mahvi & Mostafapour, 2019a, 2019b). The second problem will be solved by magnetizing the adsorbent so that it can be collected and reused with a magnet after each use of the adsorbent (Al-Musawi et al., 2021a, 2021b).

Canola with the scientific name of *Brassica napus* is one of the most important oilseeds in temperate regions and is the third most important oil plant in the world and has a relatively wide range of climatic adaptation (Balarak et al., 2015). Canola has two spring and autumn types, so it is possible to cultivate it in different climatic conditions. In Iran, oilseed of canola is cultivated in different cities due to its important properties, and its frequency is increasing every day (Balarak et al., 2015).

In most of the studies, only two Langmuir and Freundlich isotherms are used from linear models, but in this study, four types of isotherms linear and non-linear were used, which can easily identify the chemical or physical absorption of the process using the models. In most studies, equilibrium data using regression coefficients are used to match isotherms and kinetics. But employment of regression coefficient alone will not be enough for adaptability. Therefore, for more accuracy, different error coefficients were used in this study.

One of the main problems in using adsorbents for the treatment of pollutants is the reuse and recovery of adsorbents; this problem was eliminated by magnetizing the studied adsorbent so that the adsorbents were used several times, and their entry into the environment and pollution of the environment was prevented.

In this study, canola wastes were used as a raw material to produce activated carbon and then the adsorbent

was produced magnetically and it was used to remove fluoride from aqueous solutions. Also, the effect of factors affecting the process including pH, reaction time, initial fluoride concentration, and adsorbent dose and temperature were investigated in batch condition. Studies on isotherm, kinetics, and thermodynamics were also calculated. Finally, the error coefficient was calculated to determine the best isotherm and kinetics.

2 Materials and Methods

2.1 Synthesis of Materials

This research is an experimental descriptive-analytical study in which the required information was obtained by performing experiments in batch mode by applying the studied variables to the fluoride adsorption process using ACCS- Fe_3O_4 . Sodium fluoride and hydrochloric acid and sodium hydroxide, a standard reagent, and zirconium acid used were prepared by Merck Company. Also, $\text{FeCl}_2 \cdot 4\text{H}_2\text{O} \geq 99\%$ and $\text{FeCl}_3 \cdot 6\text{H}_2\text{O} 97\%$ and NH_4OH were purchased from Sigma Aldrich Co. Stock solution of 500 mg/L fluoride ions (F^-) was obtained by dissolving 1.1 g NaF in 1000 mL of double distilled water, and the concentrations used in this study were obtained by diluting the stock solution.

2.1.1 Synthesis of Fe_3O_4 Nanoparticles

Fe_3O_4 nanoparticles were prepared by chemical precipitation method. For this purpose, in a 200-mL glassware balloon, a ratio of 2 to 1 of a 0.2 M solution of $\text{FeCl}_3 \cdot 6\text{H}_2\text{O}$ and $\text{FeCl}_2 \cdot 4\text{H}_2\text{O}$ was mixed on a thermal shaker at 30 °C. Then, 10 mL of 10% NH_4OH solution was added dropwise to the solution. The reaction was performed for 1 h until the pH reached about 10 and the color of the solution changed to dark black. The precipitate was then separated using a magnet and washed several times with deionized water and immediately dried at 100 °C for 6 h and stored in a desiccator until its employment.

2.1.2 Synthesis of Activated Carbon

Canola stalks were used as raw material to produce activated carbon. Canola stalks were collected from agricultural lands. Activated carbon was prepared by physical activation of canola stalk biochar with water

vapor according to previous studies (Mahvi & Mostafapour, 2019a, 2019b).

A substrate reactor made of stainless steel located in a vertical electric furnace was used to carbonize and physically activate the rapeseed stem. For carbonization and physical activation of the canola stalk, a packed-bed reactor (made of stainless steel) located in a vertical electrical furnace was utilized. The temperature was measured by a thermocouple and controlled by an electric heater. Injection of purified N₂ (99.99%) at a continuous flow rate of 100 cm³/min through the sample was done using a mass flow controller.

First, the canola stalk was washed with distilled water to remove impurities and then dried in an oven at 120 °C overnight. Then, the dried canola stalks were crushed with a 35–60 mesh (250–500 μm) using standard ASTM sieves. The powder obtained under purified nitrogen flow was pyrolyzed from 25 to 600 °C at a heating rate of 10 °C per minute and, before cooling to 25 °C, was maintained for 2 h at 600 °C. Then, physical activation was performed using steam as the activating agent. For this process, the pyrolyzed solids were heated from laboratory temperature to 800 °C under a nitrogen flow. At 800 °C, N₂ gas was converted to water vapor and activation was performed for 1 h. Finally, the activated sample was cooled under a nitrogen gas flow.

2.1.3 Synthesis of Magnetic Activated Carbon

To magnetize the produced activated carbon, first 4 g of carbon made in the previous step was mixed with 20 mL of one molar nitric acid solution and placed in ultrasonic at 80 °C for 3 h. Then, after filtration using a 0.45-micron filter, it was dried at a temperature of 105 °C. After that, 3 g of dried activated carbon was mixed in 200 mL of deionized water with 2 g of Fe₃O₄ nanoparticles made in the first stage and placed in an ultrasound bath at 80 °C for 1 h. The adsorbent was then washed first with ethanol and then with distilled water. Finally, it was dried immediately in an oven at 100 °C for 24 h.

TEM model (LEO 912 AB) and SEM/EDX model (Mira 3-XMU) were used to determine the characteristics of prepared adsorbent. Fourier transform infrared (FT-IR) spectroscopy (Thermo Nicolet AVATAR5700) was also used in the range of 400–4000 cm⁻¹ using transmission mode on a KBr pellet. The specific surface area and the pore-size distribution were determined using a surface-area analyzer (ASAP2020,

USA), and the relevant indices were calculated by Brunauer–Emmett–Teller (BET) equation and the Barrett–Joyner–Halenda (BJH) method, respectively. The magnetic responses of ACCS-Fe₃O₄ and Fe₃O₄ were measured at room temperature using a vibrating sample magnetometer (Micromeritics Instrument Corp., Norcross, GA, USA) with an applied force between –10,000 and 10,000 Oe. Collecting the data related to X-ray diffraction (XRD) was performed with Cu-Kα irradiation ($\mu = 0.15418$ nm) at 40 kV and 40 mA and recorded in the region of 2θ between 10° and 60°.

2.1.4 Adsorption Experiments

The adsorption of F⁻ on ACCS-Fe₃O₄ was evaluated in a batch system. The parameters studied in this study include ACCS-Fe₃O₄ dose, initial fluoride concentration, initial pH, contact time, and reaction temperature. A 250-mL Erlenmeyer containing 100 mL of fluoride solution with a concentration of 5 to 50 mg/L was used for the work. In each time of the adsorption test, a certain volume of the studied F solution at a certain concentration was added to Erlenmeyer. The pH was adjusted as desired with 0.1 M NaOH or 0.1 M HCl. A certain amount of ACCS-Fe₃O₄ was added to the solution. For proper mixing and contact of the adsorbent and fluoride, an incubator shaker was used at a speed of 150 rpm for a period of 10 to 120 min and then the adsorbent was separated from the solution using a magnet. All stages of the experiment were performed in duplicate to confirm possible errors and the average of the results was represented. To prepare the calibration curve, different concentrations of fluoride were prepared using stock solution of 500 mg/L. To each of the prepared samples, 1 mL of zirconium acid reagent and 1 mL of spandns reagent were added, and after color formation, the samples were read with a DR5000 spectrophotometer at 570 nm. This curve was used to obtain unknown samples. Adsorption efficiency and mg of adsorption per g of adsorbent (q_e) were determined using the following equations. In these equations, R represents efficiency, q_e is adsorption capacity in mg/g, C₀ indicates initial concentration of fluoride in mg/L, C_e reveals concentration of fluoride in time t in mg/L, M is adsorbent mass in g, and is V sample volume in L (Zazouli et al., 2014a, 2014b; Dyanati-Tilaki et al., 2013).

$$q_e = \frac{(C_0 - C_e)}{M} \quad (1)$$

$$R = \frac{(C_0 - C_e)}{C_0} \times 100\% \quad (2)$$

3 Results and Discussion

3.1 Characterizations

The determination of magnetic properties of ACCS-Fe₃O₄ were achieved by using VSM (vibrating

sample magnetometer) analysis; this analysis for mentioned adsorbents was performed using an applied in the range of -10,000 to 10,000 Oe. For ACCS-Fe₃O₄ nanocomposite, the saturation magnetization value was 28.4 emu/g (see Fig. 1a); this value was lower than value obtained for Fe₃O₄ (bibliographically between 70 and 80 emu/g) (Al-Musawi et al., 2021a, 2021b; Yilmaz et al., 2022). Based on our obtained results, the ferromagnetic behavior detected for this nanocomposite was less compared to magnetic nanoparticles.

FTIR spectra of ACCS in the range of 400–4000 cm⁻¹, before and after its magnetic modification with iron oxide nanoparticles, are shown in Fig. 1b. The very strong adsorption peak at 3423

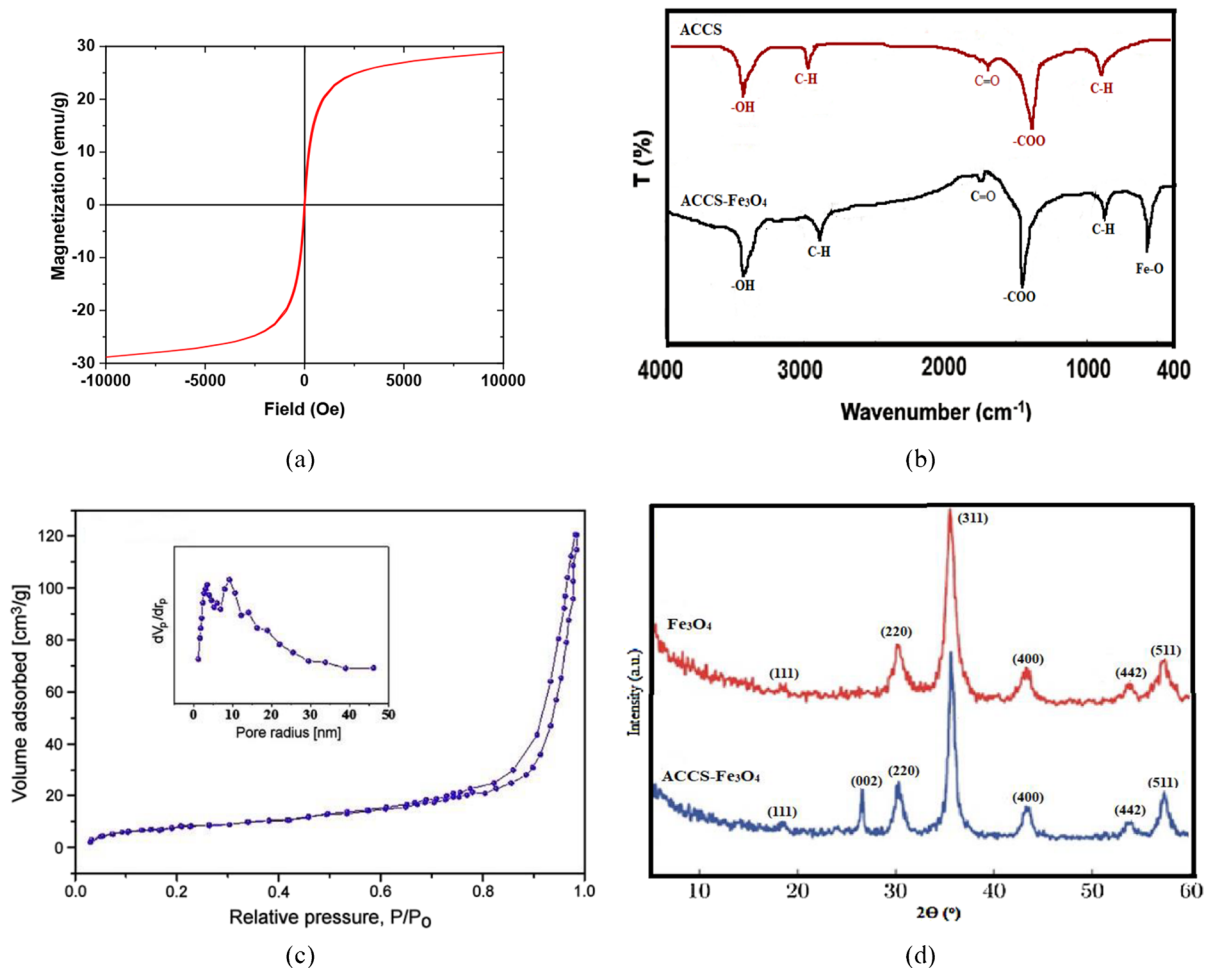


Fig. 1 **a** VSM plot of ACCS-Fe₃O₄, **b** FTIR spectra of ACCS and ACCS-Fe₃O₄, and **c** N₂ adsorption–desorption isotherms of ACCS-Fe₃O₄. Inset: pore size distributions from the adsorption branches through the BJH method. **d** XRD patterns of ACCS-Fe₃O₄

and 3426 cm^{-1} belongs to the hydroxyl groups derived from the polymeric compounds of cellulose, hemicellulose, and lignin. The bands observed in $2840\text{--}2930\text{ cm}^{-1}$ are attributed to the aliphatic CH group. The peaks in the wave numbers of $1614\text{--}1729$ and 1200 cm^{-1} represent the asymmetric stretching vibrations and the symmetric stretching vibrations of the O=C, respectively (Camacho et al., 2010). By comparing the FTIR spectra of ACCS and ACCS- Fe_3O_4 , we find that almost all of the functional groups observed in ACCS appear in ACCS- Fe_3O_4 . In addition, a new but very strong peak is observed in 590 cm^{-1} , which is related to the vibrations of the O-Fe bond in the tetrahedral positions.

BET adsorption analysis was performed to obtain more information on the surface area and pore distribution in ACCS- Fe_3O_4 . The adsorption isotherm and the pore size distribution diagram of the inset BJH of ACCS- Fe_3O_4 nanocomposites are shown in Fig. 1c. Considering the results of the N_2 adsorption-desorption isotherm measured at 77 K, type IV isotherm (in accordance to the IUPAC classification) with one clear H3-type hysteresis loop from P/P0 *0.6 to 0.9 was confirmed, which are features of mesoporous materials (Mahvi & Mostafapour, 2019a, 2019b). Specific surface area and pore volume were detected as $595.2\text{ m}^2/\text{g}$ and $0.441\text{ cm}^3/\text{g}$, respectively. The effective specific surface area and pore volume of ACCS were $642.3\text{ m}^2/\text{g}$ and $0.479\text{ cm}^3/\text{g}$, which was higher than magnetically activated carbon; this can be attributed to the overlap of carbon surfaces with iron nanoparticles. Also, the average size of ACCS- Fe_3O_4 nanocomposite is 5–30 nm with an average diameter of 11 nm.

Table SII (Supporting information section) shows the results for the properties of ACCS- Fe_3O_4 and ACCS. As it can be seen, in activated carbon and magnetic activated carbon, the main elements are carbon (43.9% and 47.1%, respectively) and oxygen (41.1% and 45.4%, respectively). After magnetization, the amount of iron in the magnetic nanocomposite increases (from 0.32 to 10.2%).

X-ray diffraction spectroscopy is a powerful technique that can be used to identify the crystal structure and phase purity of samples. Figure 1d shows the XRD patterns of pure Fe_3O_4 and ACCS- Fe_3O_4 nanocomposites. Figure 1d represents the diffraction peaks of Fe_3O_4 , which have appeared at angles of 18.5, 31.5, 35.5, 44.1, 53.6, and 57.2, which are corresponding to crystal planes of (111), (220), (311), (400), (442),

and (511); these can be indexed to the face-centered cubic lattice crystal structure model (JCPDS card no. 19–0629) of Fe_3O_4 nanoparticles. Furthermore, based on the XRD pattern, appearing characteristic peaks of carbon at 2θ of about 27° was detected; this approves the presence of amorphous carbon. Due to the intensity of the peaks and their relatively low widths, a high degree of crystallinity can be detected in nanocomposite (Mahvi & Mostafapour, 2019a, 2019b). In this spectrum, using Debye–Scherrer equation, the size of Fe_3O_4 nanoparticles was calculated to be 8.36 nm and for ACCS- Fe_3O_4 nanocomposite, it was calculated to be 9.5 nm. The mentioned results confirm the results obtained from the BJH analysis. The Debye–Scherrer equation (Eq. 3) is written as follows (Laura et al., 2015):

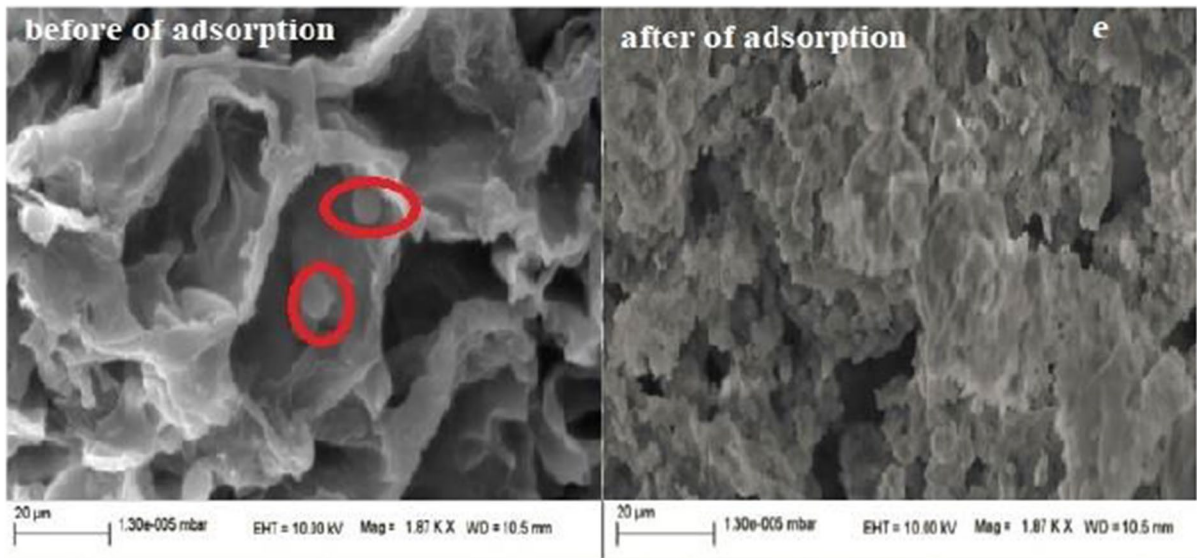
$$D = \frac{0.9\lambda}{\beta \cdot \cos\theta} \quad (3)$$

where D is the crystal particle size, λ is the X-ray wavelength, β is the width of the background peak at half height, and θ is the Bragg angle.

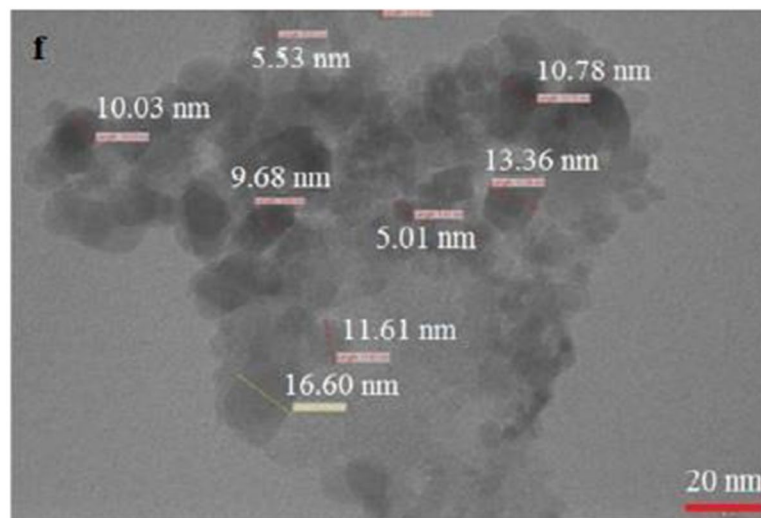
Figure 2a shows the SEM image before and after fluoride adsorption. As can be seen, the white spots on the adsorbent represent the iron nanoparticles. As well, the large pores and cavities can be seen in the figure, which are covered by fluoride molecules. TEM images of ACCS- Fe_3O_4 nanocomposite are shown in Fig. 2b; in this figure, TEM images show the size and shape of the magnetic nanocomposite and it can be seen that the iron oxide nanoparticles are located in the pores of the carbon matrix and the size of the nanocomposite is in the range of 5 to 17 nm.

3.2 Adsorption Evaluation

Determining the effect of adsorbent dose due to its effect on the economics of the adsorption process for the design of large commercial-industrial systems is one of the most important issues in these systems. Experiments were performed at pH equal to 5 at an initial fluoride concentration of 25 mg/L at contact time of 60 min and at 30 °C. As shown in Fig. 3a, although increasing the dose of ACCS- Fe_3O_4 leads to an increase in fluoride removal efficiency, this increase leads to a decrease in fluoride adsorption per unit mass of adsorbent. By increasing the adsorbent dose from 0.1 to 0.6 g, the removal rate increases, but by increasing the



(a)



(b)

Fig. 2 a SEM images of ACCS-Fe₃O₄ (before and after adsorption). b TEM images of ACCS-Fe₃O₄

adsorbent dose to values higher than 0.6 g/L, not only there is no noticeable positive change in the removal rate, but also the removal rate decreases slightly. The cause of this phenomenon can be related to the unsaturation of some sites on the surface, which results in reduced adsorption. The increase in removal efficiency is due to the increase in the available surface in the system, but the decrease in the amount of contaminant adsorbed per adsorbent mass is due to the fact that the

increase in adsorbent mass leads to overlap of adsorbent surfaces and their accumulation resulting in reduced useful surface area (Sani et al., 2016). Also, increasing the adsorbent dose and their accumulation increases the diffusion path during the pollutant diffusion phase at the adsorbent surfaces, which will result in a decrease in the adsorption rate. On the other hand, in such conditions, due to the competition between the pollutant molecules in occupying the empty adsorbent surfaces,

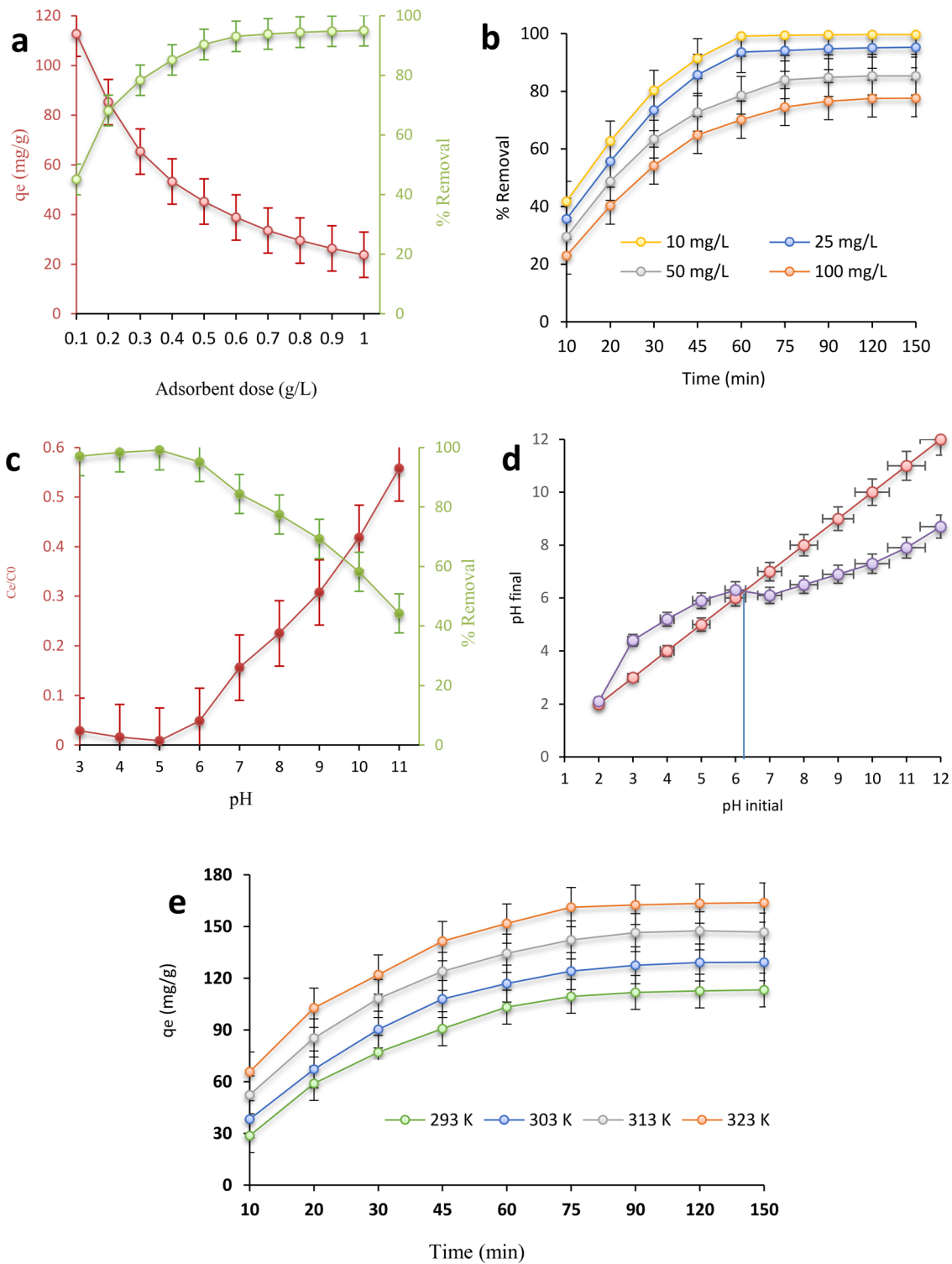


Fig. 3 a Effect of adsorbent's dose on fluoride removal. b Effect of initial fluoride concentration. c Effect of pH on fluoride removal. d Determination of pH_{ZPC} . e Effect of tempera-

ture on fluoride uptake by ACCS- Fe_3O_4 . A nominal value of 5% is recommended in statistical studies, so this value was included in error bars

the adsorbent surfaces are used in unsaturated state and all its capacities are not used optimally, which results in reducing the amount of pollutant adsorbed per unit mass of adsorbent (Zúñiga-Muro et al., 2014). Therefore, determining the optimal dose to prevent unwanted loss of the adsorbent is very important.

Determining the effect of the initial concentration of contaminants entering the adsorption systems is one of the most important parameters that should be considered in adsorption systems. Experiments were performed at pH equal to 5 at an adsorbent dose of 0.6 g/L at 30 °C and contact time between 10 and 150 min. The results of this study showed that in the initial fluoride concentration of 10 mg/L, the amount of adsorption is the highest possible amount among the studied concentrations, but in higher initial concentrations, the removal efficiency decreases (Fig. 3b). At lower fluoride concentrations, adsorption occurs at the inlet areas of the pore or near the inlet portion of the pore, which adsorption is faster and with a larger amount due to the short diffusion path in this case and the presence of sufficient space to adsorb a certain amount of pollutants, while in higher concentrations, these areas are saturated faster and more adsorption requires penetration into deeper pore areas through penetration or crossing a relatively long path that these conditions lead to a decrease in the amount of adsorption and the rate of adsorption at a given time (Leyva-Ramos et al., 2010; Yami et al., 2016). Figure 3b shows also the effect of contact time on the fluoride adsorption efficiency by ACCS-Fe₃O₄. As it can be seen, with increasing contact time, the efficiency of fluoride adsorption from the aqueous solution increases. For different concentrations in the early times, the intensity of adsorption is very high, but over time, the changes slow down until it finally reaches a constant value, which is called the equilibrium time. Equilibrium time at concentrations of 10 and 25 mg/L was obtained equal to 60 min and for concentrations 50 and 100 mg/L was equal to 75 min. After reaching equilibrium time, the amount of fluoride ions adsorbed did not change much over time. Increasing the removal efficiency is due to the fact that with increasing time, there is more opportunity for the adsorbent to contact and adsorb the fluoride ions. The high rate of fluoride adsorption in the early stages is due to the availability of more vacant active sites on the adsorption surface. These sites are filled and the adsorbent is saturated, and after equilibration of the adsorbent, the adsorption process may be due to the limited transfer of mass from

the liquid medium to the adsorbent surface (Brunson & Sabatini, 2009).

One of the most important environmental factors affecting the adsorption of contaminants on the adsorbent surface is the distribution of positive and negative surface charges on the adsorbent surface, which is a function of the pH of the reaction medium. This factor affects the adsorption of different pollutants at different surfaces by changing the balance of electrical charges. Accordingly, it is necessary to determine the effect of this parameter on the adsorption of various contaminants by adsorbents. Experiments were performed at adsorbent dose equal to 0.6 g/L at initial F⁻ concentration of 10 mg/L at contact time of 60 min and at 30 °C. The results of this study in Fig. 3c show that changing the pH of the environment and increasing it from 3 to 5 increase the amount of fluoride adsorption, and by increasing the pH to 11, the efficiency again increases. The cause of this phenomenon is related to the anionic structure of fluoride and p_{H_{ZPC}} for ACCS-Fe₃O₄. Studies show that at pH equivalent to p_{H_{ZPC}}, the electric charges on the adsorbent surface are balanced, but at pH higher and lower than p_{H_{ZPC}}, the dominant surface electric charge is negatively or positively present on the adsorbent surface, which these conditions along with the anionic or cationic conditions of the contaminant affect the removal efficiency (Loganathan et al., 2013; Wongrueng et al., 2016). Based on the results of this study that p_{H_{ZPC}} for ACCS-Fe₃O₄ was equal to 6.1 (Fig. 3d); it can be said that at pH above 6.1, the predominant surface area of ACCS-Fe₃O₄ is negative, which is due to the accumulation of hydroxyl anions in the adsorbent surface and increase in number of negative charges. Due to the fact that fluoride is also anionic in nature, the result is thought to be that the removal efficiency is reduced due to the similarity of surface charge, and at pH of 11, the removal efficiency reaches 44%. Because the anionic nature of fluoride on the one hand and increasing the pH of the environment, which confirms the accumulation of negative electrical charges on the adsorbent surface, leads to a repulsion between the adsorbent and the contaminant, this consequently leads to a decrease in fluoride adsorption efficiency (Akbari et al., 2018).

Temperature is another factor affecting the rate of adsorption, which plays an important role in the process of fluoride adsorption by ACCS-Fe₃O₄.

To investigate the effect of temperature on fluoride adsorption, several experiments were performed under the same conditions at different temperatures of 293, 303, 313, and 323 K; the results of which are shown in Fig. 3e. As it can be seen, with increasing temperature, the amount of adsorption increases, which means that the fluoride adsorption process on ACCS-Fe₃O₄ is endothermic (Yadav et al., 2018; Yilmaz et al., 2022). In addition, for this experiment, the adsorbent dosage of 0.6 g/L, pH=5, F⁻ concentration of 100 mg/L, and contact time between 10 and 150 min were considered.

To estimate the thermodynamic parameters, i.e., free energy change (ΔG^0), enthalpy change (ΔH^0), and entropy change (ΔS^0), the equations represented below were employed (Al-Musawi et al., 2021a, 2021b; Kanouo et al., 2020).

$$\Delta G^0 = -R \cdot T \cdot \ln(K_c) \quad (4)$$

$$\ln(K_c) = \frac{\Delta S^0}{R} - \frac{\Delta H^0}{RT} \quad (5)$$

where K_c is representative of the sorption equilibrium constant; R indicates the gas constant, and T was indicative of the absolute temperature (K).

The estimation of ΔH^0 and ΔS^0 was achieved by using the slope and the intercept of the Eq. (5), which are obtained by drawing $\ln(K_c)$ versus $1/T$ (Fig. S11). In Table 1, the calculated values of ΔG^0 , ΔS^0 , and ΔH^0 were presented. The positive value was observed for ΔH^0 , which is indicative of the endothermic nature of the F⁻ sorption; it is consistent with the findings of the isotherm Temkin model.

For the studied adsorption process, the positive values were achieved for ΔS^0 ; this indicates that during the adsorption process, we are faced with the randomness at solid/solution interface (Yilmaz et al., 2022). Additionally, the negative values were calculated for ΔG^0 ; this is indicative of spontaneous nature of adsorption. Increasing the temperature was associated with increasing the negativity of ΔG^0 values, which means the feasibility of the sorption of F⁻ ions by increasing temperature (Alhassan et al., 2020).

3.3 Modeling

3.3.1 Determination of Adsorption Isotherms

Adsorption isotherms are mathematical equations to describe the amount of adsorption and equilibrium

Table 1 Thermodynamic parameters for the adsorption of F⁻ on ACCS-Fe₃O₄

T (K)	ΔG^0 (kJ/mol)	ΔH^0 (kJ/mol)	ΔS^0 (kJ/mol K)
293	-2.78	69.3	0.244
303	-3.92		
313	-5.81		
323	-10.31		

state of the adsorbent between solid and fluid phases. In studies related to the adsorption of pollutants on different adsorbents, determining the adsorption isotherm and adsorbent capacity is the most important feature used to estimate the performance of systems. Experimental data on adsorption equilibrium were analyzed by Langmuir, Freundlich, Temkin, and D—R adsorption isotherm models. To check the agreement of the data with these absorption models, linear and nonlinear states of the general equations of these models were used; the equations of which are shown in Table S12 (Fito et al., 2019). The expression of adsorption equilibrium using only regression coefficient will be accompanied by error; thus, to improve the work process and ensure the results obtained from kinetics and isotherms, error coefficient is used. In this study, four error coefficients were used to determine the best type of isotherm and kinetics, in addition to regression coefficient. These four error coefficients were the sum of square error (Eq. 6), non-linear-chi-square test (Eq. 7), hybrid fractional error functions (Eq. 8), and Marquardt's percent standard deviation (Eq. 9) (Prabhu and Meenakshi, 2014):

$$SSE = \sum_{i=1}^n (q_{e,cal} - q_{e,exp})^2 \quad (6)$$

$$x^2 = \sum_{i=1}^n \frac{(q_{e,cal} - q_{e,exp})^2}{q_{e,cal}} \quad (7)$$

$$HYBRID = \sum_{i=1}^n \left[\frac{(q_{e,cal} - q_{e,exp})^2}{q_{e,exp}} \right] \quad (8)$$

$$MPSD = \sum_{i=1}^n \left[\frac{(q_{e,exp} - q_{e,cal})^2}{q_{e,exp}} \right] \quad (9)$$

Linear regression analysis and the least squares are methods, which are regularly used for the best fitting and finding the parameters of isotherms; in this study, Langmuir, Freundlich, Temkin, and D-R isotherms (in their linear forms provided in Table SI2 (Supporting information section)) were used for this purpose, as well as, for describing the relationship between the amount of F^- adsorbed q_e and its equilibrium concentration (C_e).

According to coefficient of determination values (R^2) shown in Table SI3 (Supporting information section) and Fig. 4a–d, the Langmuir model with highest R^2 was the best model for describing adsorption of F^- onto ACCS- Fe_3O_4 adsorbent; this is indicative of existing strong evidence for obedience of the sorption of the chosen F^- onto the ACCS- Fe_3O_4 from the Langmuir isotherm. A maximum capacity of 161.2 mg/g has been obtained for this model compared to the other types of the model according to R^2 values and related SSE, χ^2 , HYBRID, and MPSD. However, the error function was observed to be lower for the Langmuir. This best fitting is due to the minimal deviations from the fitted equation resulting in the best error distribution.

To escape from errors caused by different estimates resulting from simple linear regression of the linearized forms of isotherm models presented in Table SI3 (Supporting information section), which have significant effect on statistical parameters (R^2 , SSE, χ^2 , HYBRID, and MPSD) values, the use of non-linear analysis is common. For this purpose, the use of non-linear analysis is considered as an adequate method, which is a fascinating approach for explanation of adsorption isotherms employed for many applications, e.g., wastewater treatment. The nonlinear analysis of Langmuir and Freundlich, Temkin, and D-R adsorption isotherms for adsorption of fluoride by ACCS- Fe_3O_4 and their corresponding isotherm parameters, coefficients of determination (R^2), and related standard errors for each parameter are represented and summarized in Table SI3 (Supporting information section) and Fig. 4e. Fitting experimental data into the Langmuir isotherm model could provide higher values of R^2 in this study. Furthermore, lower values of SSE, χ^2 , HYBRID, and MPSD were achieved for each parameter obtained in Langmuir models with higher R^2 , which is suggestive of a satisfactory fit with the experimental data. Also, the amount of R_L in the linear and non-linear Langmuir equation was between zero and one, which indicates

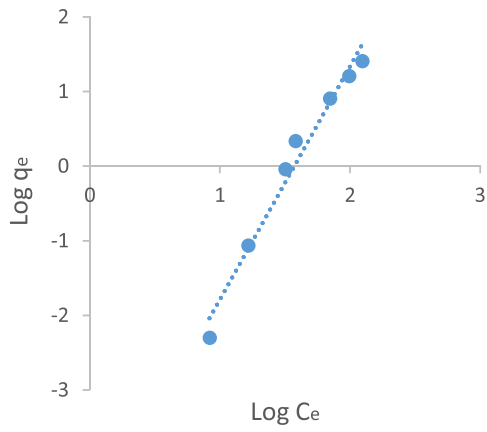
the confirmation of absorption by the Langmuir isotherm. Also, the amount of energy E from the D-R in both linear and nonlinear methods was less than 8 kJ/mol, which indicates the physical absorption of fluoride by the studied adsorbent.

The potential use of new adsorbents on an industrial scale depends on the adsorbent capacity compared to other adsorbents in pollutant adsorption. The adsorption capacity values of other adsorbents for fluoride removal are shown in Table 2. It is clear that the adsorption capacity of ACCS- Fe_3O_4 is reported to be significantly higher or comparable to that of many low-cost adsorbents of literature. In addition, the fluoride removal efficiency using ACCS- Fe_3O_4 was higher than of non-magnetized ACCS, and this result indicating the role of Fe_3O_4 nanoparticles in the increasing of ACCS capacity for fluoride adsorption.

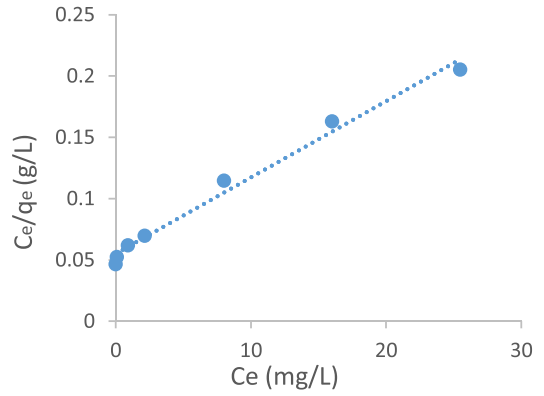
3.3.2 Determination of Adsorption Kinetics

The initial adsorption behavior was analyzed based on the Weber and Morris equation or the intraparticle diffusion model (IPD) shown in the linear equation (Table SI2 (Supporting information section)). This model is usually used in three forms: (a) the first form is to obtain a straight line diagram that is forced to pass through the origin; (b) The second figure is a multi-linear design with two or three steps, including the whole process as follows: external adsorption or instantaneous adsorption occurs in the first step, and the second step is the gradual adsorption in which IPD is controlled, and the third stage is the final equilibrium in which the solutes are slowly transferred from the larger pores to the finer pores at a lower adsorption rate; and (c) the third form is that a straight line is obtained but does not necessarily cross the origin. That is, there is an intercept (Varaprasad et al., 2018). Intercept is proportional to the amount of boundary layer thickness; the larger intercept is indicative of the greater effect of the boundary layer. As it can be seen in Fig. 5a and Table SI5 (Supporting information section), fluoride adsorption by ACCS- Fe_3O_4 is composed of three separate steps.

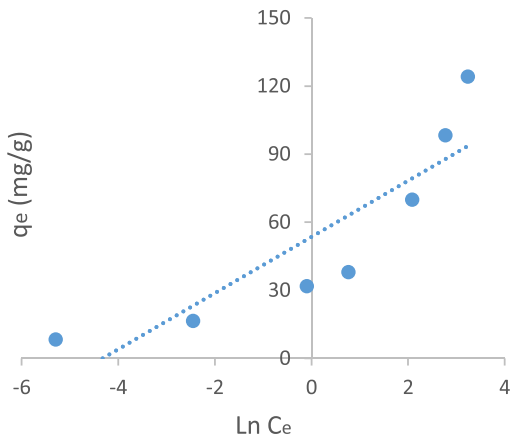
The first step occurs in 10 to 30 min when the adsorption rate is high and the adsorption rate or $k_d I$ is high. Adsorption occurs at adsorbent surface points (bulk diffusion). In the second stage, which occurs from 30 to 60 min, the slope of the graph is reduced



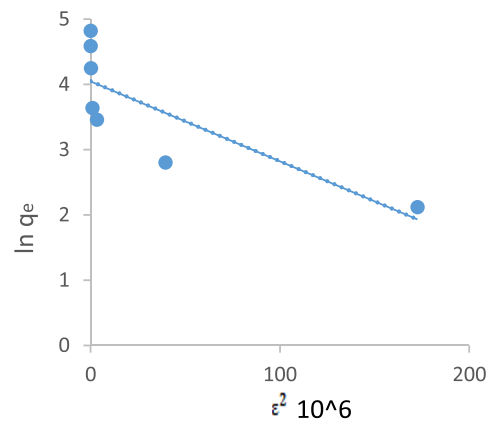
(a)



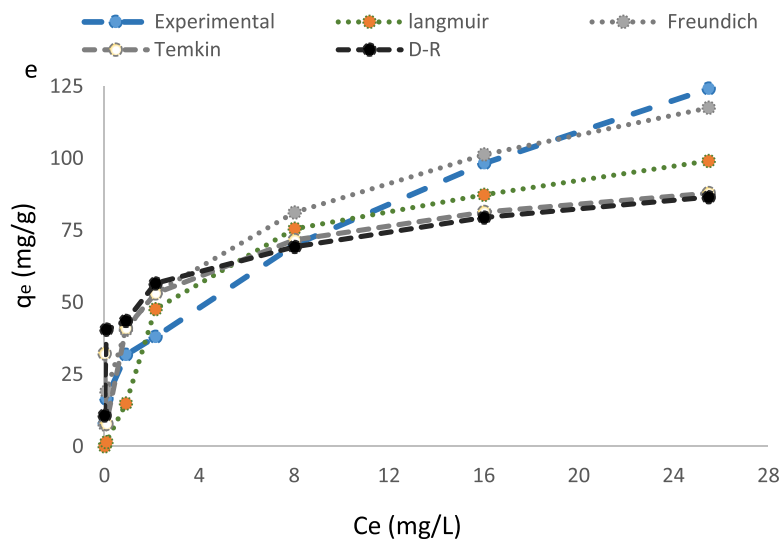
(b)



(c)



(d)



(e)

Fig. 4 Adsorption isotherms for fluoride removal by Fe₃O₄-CSAC: **a** linear-Freundlich, **b** linear-Langmuir, **c** linear-Temkin, **d** linear-D-R, **e** nonlinear isotherms

and therefore the adsorption rate is lower and arises from the penetration of contaminants from the surface layers to the absorbent depth and it can be seen that k_{p2} is less than k_{p1} (film diffusion).

The third stage, which is very low speed and can be ignored, occurs from 60 min onwards; the slope of the third stage diagram is very low and occurs from penetration into the small pores inside the adsorbent (pore diffusion) (Khandare & Mukherjee, 2019).

The adsorption kinetics in this study were performed using linear and non-linear pseudo first order (PFO) and PSO kinetic models. The equations for the kinetics are given in Table SI2 (Supporting information section). As it can be shown from the results of the kinetics in Table SI5 (Supporting information section) and Fig. 5b–e, in all the studied errors, the equilibrium data with respect to the high regression coefficient and the error coefficient follow less than the second-order kinetics. Also, the q_e obtained from the PSO kinetic model is more compatible with the experimental q_e , but for the PFO kinetics, the computational and experimental q_e do not match and have a great difference; thus, it can be said that considering high regression coefficients, lower error coefficients, and greater adaptation of computational and laboratory q_e , equilibrium data follow PSO kinetics.

Table 2 The comparison of adsorption capacity of different adsorbents for fluoride removal

Adsorbent	Q_e , (mg/g)	Ref
Lemna minor	51.3	(Zazouli et al., 2014a, 2014b)
Neem leaf powder	34.6	(Bharali et al., 2015)
MgO nanoparticle	64.1	(Zhen et al., 2016)
Eggshell powder	56.4	(Bhaumik et al., 2012)
CuO nanoparticle	38.7	(Bazrafshan et al., 2016)
MWCNT	71.2	(Balarak et al., 2016)
Nano-alumina	65.1	(Kumar et al., 2011)
Montmorillonite	45.2	(Tor, 2006)
Granular ceramic	73.2	(Chen et al., 2010)
Sorghum	36.8	(Zazouli et al., 2015)
<i>Azolla filiculoides</i>	41.9	(Zazouli et al., 2014a, 2014b)
ACCS	74.9	This work
ACCS-Fe ₃ O ₄	161.2	This work

3.4 Reuse and Influence of Co-existing Ions

We also used ACCS-Fe₃O₄ to test reusability and stability, which is important in terms of cost-effectiveness, design, and practicality. Reusability tests were performed for six consecutive cycles under optimal conditions. After each cycle, desorption was performed by washing the adsorbent with ethanol and subsequently with distilled water, then the washed material was dried until complete dryness. The adsorption efficiency of ACCS-Fe₃O₄ after any recycling is shown in Fig. 6a. No significant decrease in Fe₃O₄-ACCS adsorption capacity was observed. The adsorption percentage only decreased from 100 (first recycling) to 92.1% (sixth recycling); this proves the high reusability and ACCS-Fe₃O₄ for six recycling, which satisfies both economic and practical aspects. The observed slight decrease in adsorption efficiency after six cycles can be attributed to the loss in the adsorption sites during washing and drying processes (Kennedy & Arias-Paic, 2020).

Drinking water contains several other ions, especially anions. These anions, like fluoride, tend to be adsorbed on the adsorbent, so they change the adsorption capacity of the adsorbent (Alkurdi et al., 2019). Therefore, we are interested in this section to study their effects on defluoridation. Adsorption experiments were performed in the presence of initial concentrations (10 mg/L) of SO₄²⁻, Cl⁻, CO₃²⁻, and NO₃⁻ ions, while other parameters were constant. As shown in Fig. 6b, the percentage of adsorption decreases with the addition of other ions. These results can be explained by the fact that these ions replace fluoride ions at the adsorption sites and are therefore adsorbed by ACCS-Fe₃O₄. The same result was reported in the work of Zhijie et al. (2011), who investigated the effect of bicarbonate ions on the removal of fluoride ions at different concentrations. They noticed a decrease in the removal of fluoride ions in the presence of bicarbonate ions. This decrease may be due to the competition of bicarbonate ions for active sites at the adsorbent surface.

4 Conclusions

In this study, fluoride removal was investigated using activated carbon prepared from canola stalk and magnetized with iron nanoparticles (Fe₃O₄). The results

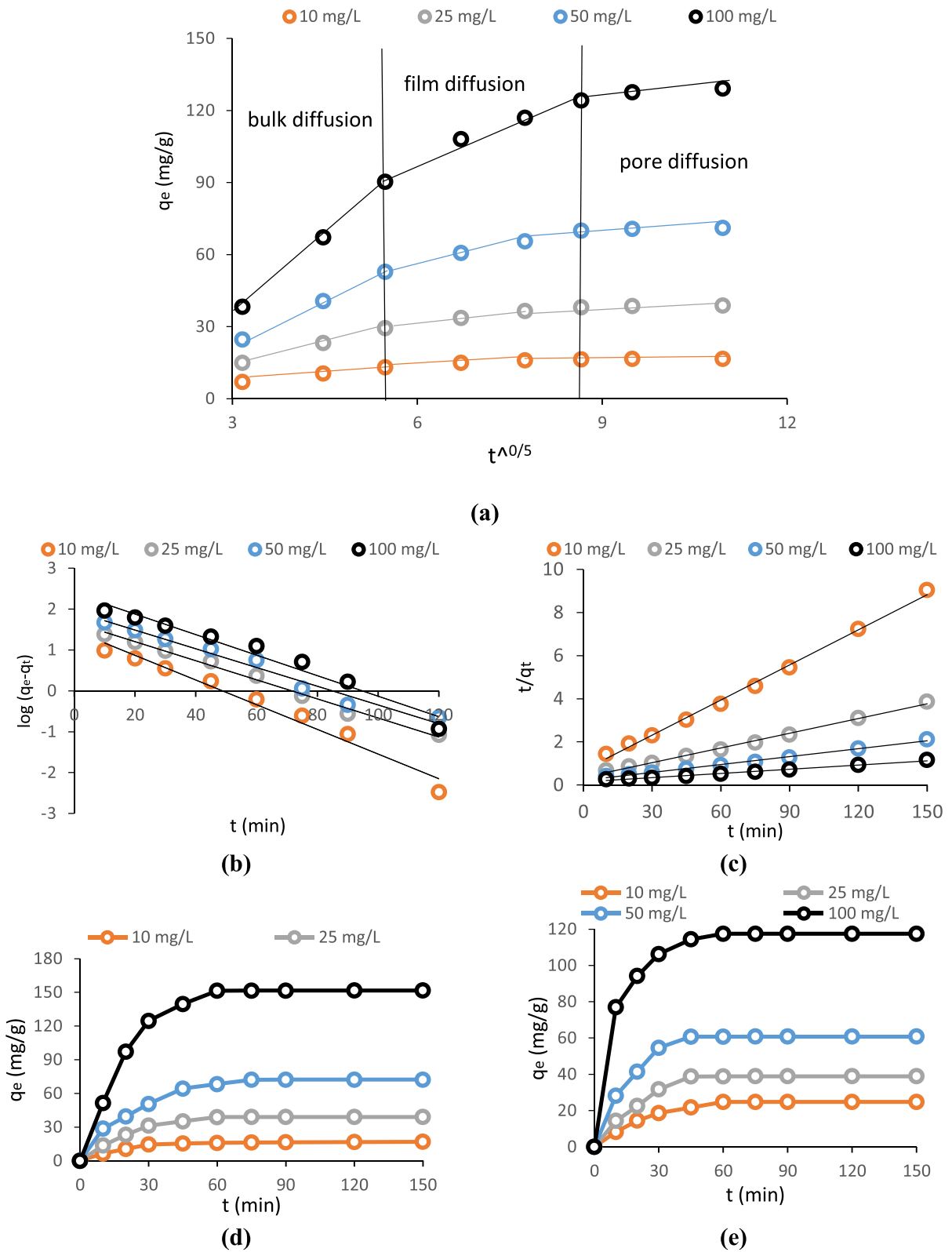
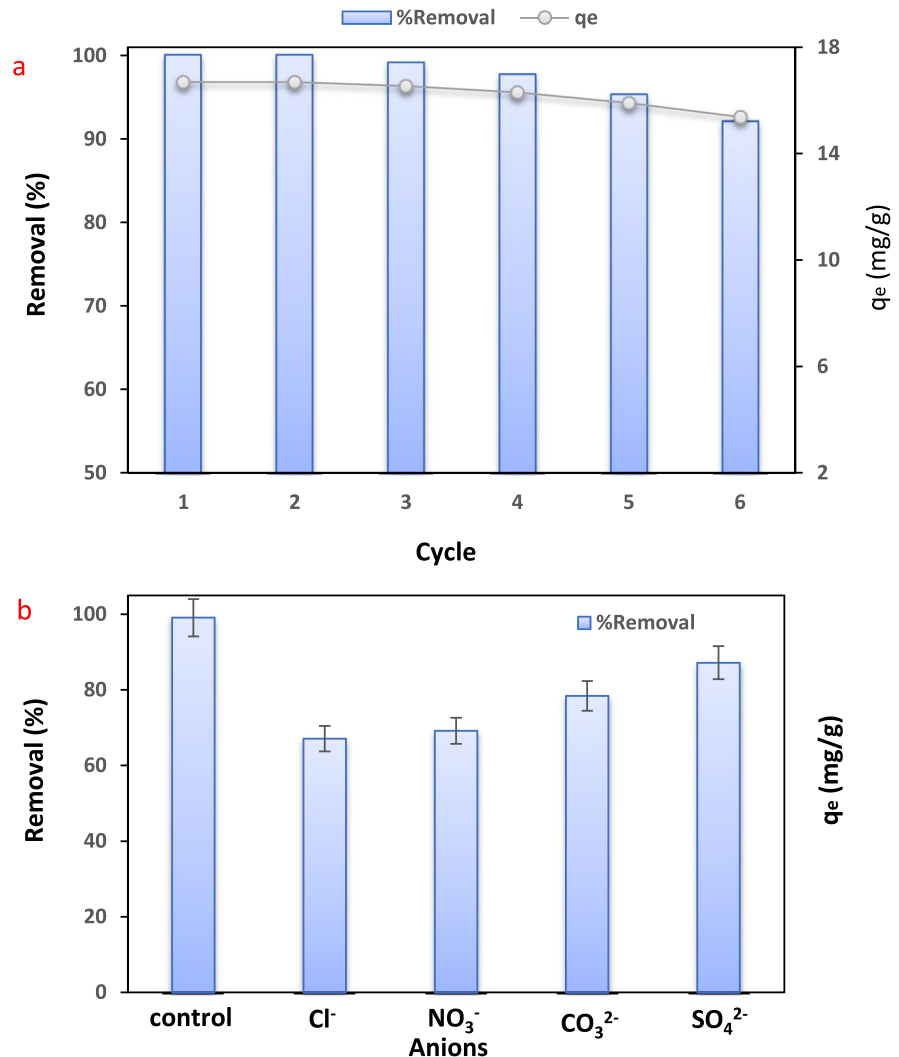


Fig. 5 Adsorption kinetics for fluoride removal: a linear PFO, b linear PSO, c nonlinear PFO, d nonlinear PSO

Fig. 6 a Reuse cycles (adsorption–desorption) of ACCS-Fe₃O₄ (control means there is no anion in the aqueous solution). **b** Influence of co-existing ions on fluoride uptake (b) ($C_0=10$ mg/L, temperature 30 ± 2 °C, dose = 0.6 g/L, and time 60 min, pH = 5)



showed that ACCS-Fe₃O₄ with high efficiency has the ability to remove maximum fluoride in a short time. According to the results, with increasing the adsorbent dose and reaction time and temperature, the removal efficiency increases and the adsorption process was endothermic and spontaneous according to thermodynamic studies. The experimental results showed that the pH of 5, the adsorbent of 0.6 g/L, and the time of 60 min were the optimal conditions for the removal of 10 mg/L fluoride at a laboratory temperature of 30 °C, which is equal to 100%. Of the four isotherm models studied, the Langmuir isotherm in both linear and nonlinear models was more consistent with equilibrium data because it had a higher regression coefficient and a lower error coefficient

than the other models. Adsorption recycling showed its high efficiency, and therefore, due to the wide range of applications of activated carbon powder in the removal of various organic and toxic pollutants from aqueous media, its magnetization by the method used in the present study (with the aim of accelerating the separation process) can be used as an economical, efficient, and reliable method.

Funding We are grateful to the student research committee of Zahedan University of Medical Sciences for their financial support.

Data Availability The data that support the findings of this study are available from the corresponding author upon reasonable request.

Declarations

Conflict of Interest The authors declare no competing interests.

References

- Akbari, H., Jorfi, S., Mahvi, A. H., & Yousefi, M. (2018). Adsorption of fluoride on chitosan in aqueous solutions: Determination of adsorption kinetics. *Fluoride*, 51(4), 319–327.
- Alhassan, S. I., Huang, L., He, Y., Yan, L., Wu, B., & Wang, H. (2020). Fluoride removal from water using alumina and aluminum-based composites: A comprehensive review of progress. *Critical Reviews in Environmental Science and Technology*, 2020, 1–35.
- Alkurdi, S. S., Al-Juboori, R. A., Bundschuh, J., & Hamawand, I. (2019). Bone char as a green sorbent for removing health threatening fluoride from drinking water. *Environment International*, 2019(127), 704–719.
- Al-Musawi, T. J., Mengelizadeh, N., & Taghavi, M. (2021). Activated carbon derived from *Azolla filiculoides* fern: A high-adsorption-capacity adsorbent for residual ampicillin in pharmaceutical wastewater. *Biomass Conversion and Biorefinery*. <https://doi.org/10.1007/s13399-021-01962-4>
- Al-Musawi, T. J., McKay, G., Kadhim, A., & Joybari, M. (2022). Activated carbon prepared from hazelnut shell waste and magnetized by Fe₃O₄ nanoparticles for highly efficient adsorption of fluoride. *Biomass Conversion and Biorefinery*. <https://doi.org/10.1007/s13399-022-02593-z>
- Balarak, D., Jaafari, J., Hassani, G., & Agarwal, G. V. K. (2015). The use of low-cost adsorbent (Canola residues) for the adsorption of methylene blue from aqueous solution: Isotherm, kinetic and thermodynamic studies. *Colloid and Interface Science Communications*, 7, 16–19.
- Balarak, D., Mahdavi, Y., Bazrafshan, E., Mahvi, A. H., & Esfandyari, Y. (2016). Adsorption of fluoride from aqueous solutions by carbon nanotubes: Determination of equilibrium, kinetic, and thermodynamic parameters. *Fluoride*, 49(1), 71–83.
- Balarak, D., Mostafapour, F. K., Bazrafshan, E., & Mahvi, A. H. (2017). The equilibrium, kinetic, and thermodynamic parameters of the adsorption of the fluoride ion on to synthetic nano sodalite zeolite. *Fluoride*, 50(2), 17–25.
- Bazrafshan, E., Balarak, D., Panahi, A. H., & Kamani, H. (2016). Fluoride removal from aqueous solutions by cupric oxide nanoparticles. *Fluoride*, 49(3), 233–44.
- Bhan, C., Singh, J., & Sharma, Y. C. (2022). Synthesis of lanthanum-modified clay soil-based adsorbent for the fluoride removal from an aqueous solution and groundwater through batch and column process: Mechanism and kinetics. *Environment and Earth Science*, 81, 253. <https://doi.org/10.1007/s12665-022-10377-x>
- Bharali, R., Bhattacharyya, K., & Krishna, G. (2015). Biosorption of fluoride on Neem (*Azadirachta indica*) leaf powder. *Journal of Environmental Chemical Engineering*, 3(2), 662–669.
- Bhaumik, R., Mondal, N. K., Das, B., Roy, P., Pal, K. C., & Datta, J. K. (2012). Eggshell powder as an adsorbent for removal of fluoride from aqueous solution: Equilibrium, kinetic and thermodynamic studies. *Journal of Chemistry*, 9, 1457–1480.
- Borgohain, X., & Rashid, H. (2022). Rapid and enhanced adsorptive mitigation of groundwater fluoride by Mg(OH)₂ nanoflakes. *Environmental Science and Pollution Research*. <https://doi.org/10.1007/s11356-022-20749-2>
- Brunson, L. R., & Sabatini, D. A. (2009). An evaluation of fish bone char as an appropriate arsenic and fluoride removal technology for emerging regions. *Environmental Engineering Science*, 26, 1777–1783.
- Camacho, L. M., Torres, A., Saha, D., & Deng, S. (2010). Adsorption equilibrium and kinetics of fluoride on sol-gel-derived activated alumina adsorbents. *Advances in Colloid and Interface Science*, 349, 307–313.
- Chen, N., Zhang, Z., Feng, C., Sugiura, N., Li, M., & Chen, R. (2010). Fluoride removal from water by granular ceramic adsorption. *Advances in Colloid and Interface Science*, 2010(348), 579–584.
- Choi, M. Y., Lee, C. G., & Park, S. J. (2022). Conversion of organic waste to novel adsorbent for fluoride removal: Efficacy and mechanism of fluoride adsorption by calcined *Venerupis philippinarum* Shells. *Water, Air, & Soil Pollution*, 233, 281. <https://doi.org/10.1007/s11270-022-05757-9>
- Dyanati-Tilaki, R. A., Yousefi, Z., & Yazdani-Cherati, J. (2013). The ability of azollaand lemna minor biomass for adsorption of phenol from aqueous solutions. *Journal of Mazandaran University of Medical Sciences*, 23(106), 140–146.
- Fito, J., Said, H., Feleke, S., & Worku, A. (2019). Fluoride removal from aqueous solution onto activated carbon of *Catha edulis* through the adsorption treatment technology. *Environmental Systems Research*, 8, 1–10.
- Haghighat, G. A., Dehghani, M. H., & Nasser, S. (2012). Comparison of carbon nanotubes and activated alumina efficiencies in fluoride removal from drinking water. *Indian Journal of Science and Technology*, 5(23), 2432–2435.
- Jadhav, S. V., Bringas, E., Yadav, G. D., Rathod, V. K., Ortiz, I., & Marathe, K. V. (2015). Arsenic and fluoride contaminated groundwaters: A review of current technologies for contaminants removal. *Journal of Environmental Management*, 162, 306–325.
- Joshi, S., Garg, M., & Jana, S. T. (2022). Hermal activated adsorbent from sawdust for fluoride removal: Batch study. *Journal of The Institution of Engineers (India): Series e*. <https://doi.org/10.1007/s40034-022-00244-6>
- Kanouo, B. M. D., Fonteh, M. F., & Ngambo, S. P. (2020). Development of a low cost household bone-char defluoridation filter. *International Journal of Biological and Chemical Sciences*, 14, 1921–1927.
- Kennedy, A. M., & Arias-Paic, M. (2020). Fixed-bed adsorption comparisons of bone char and activated alumina for the removal of fluoride from drinking water. *Journal of Environmental Engineering*, 146, 04019099.
- Khandare, D., & Mukherjee, S. A. (2019). Review of metal oxide nanomaterials for fluoride decontamination from water environment. *Materials Today: Proceedings*, 18, 1146–1155.
- Kumar, E., Bhatnagar, A., Kuma, R. U., & Sillanpaa, M. (2011). Defluoridation from aqueous solutions by nano-alumina: Characterization and sorption studies. *Journal of Hazardous Materials*, 186, 1042–9.

- Laura, C., Lisa, S., & Decker, D. (2015). Comparing activated alumina with indigenous laterite and bauxite as potential sorbents for removing fluoride from drinking water in Ghana. *Applied Geochemistry*, 56, 50–66.
- Leyva-Ramos, R., Rivera-Utrilla, J., Medellin-Castillo, N., & Sanchez-Polo, M. (2010). Kinetic modeling of fluoride adsorption from aqueous solution onto bone char. *Chemical Engineering Journal*, 158, 458–467.
- Li, Y. H., Wang, S., Cao, A., Zhao, D., Zhang, X., Xu, C., & Luan, Z. (2010). Adsorption of fluoride from water by amorphous alumina supported on carbon nanotubes. *Chemical Physics Letters*, 350, 412–416.
- Loganathan, P., Vigneswaran, S., Kandasamy, J., & Naidu, R. (2013). Defluoridation of drinking water using adsorption processes. *Journal of Hazardous Materials*, 248–249, 1–19.
- Mahvi, A. H., & Mostafapour, F. K. (2019a). Adsorption of fluoride from aqueous solutions by a chitosan/zeolite composite. *Fluoride*, 52(4), 546–552.
- Mahvi, A. H., & Mostafapour, F. K. (2019b). Adsorption of fluoride from aqueous solution by eucalyptus bark activated carbon: Thermodynamic analysis. *Fluoride*, 52(4), 562–568.
- Mohammadi, A. K., Yousefi, M., Yaseri, M., & Jalilzadeh, M. (2017). Skeletal fluorosis in relation to drinking water in rural areas of West Azerbaijan, Iran. *Scientific Reports*, 173(7), 44–51.
- Prabhu, S. M., & Meenakshi, S. (2014). Synthesis of metal ion loaded silica gel/chitosan biocomposite and its fluoride uptake studies from water. *Journal of Water Process Engineering*, 3, 144–150.
- Premathilaka, R. W., & Liyanagedera N. D. (2019). Fluoride in drinking water and nanotechnological approaches for eliminating excess fluoride. *Journal of Nanotechnology*, 2019, 2192383.
- Rahmani, A., Rahmani, K., Dobaradaran, S., Mahvi, A. H., Mohamadjani, R., & Rahmani, H. (2010). Child dental caries in relation to fluoride and some inorganic constituents in drinking water in Arsanjan, Iran. *Fluoride*, 43(4), 179–186.
- Sani, T., Gómez-Hortigüela, L., Perez-Pariente, J., Chebude, Y., & Diaz, I. (2016). Defluoridation performance of nano-hydroxyapatite/stilbite composite compared with bone char. *Separation and Purification Technology*, 157, 241–248.
- Somak, C., & Sirshendu, D. (2014). Adsorptive removal of fluoride by activated alumina doped cellulose acetate phthalate (CAP) mixed matrix membrane. *Separation and Purification Technology*, 125, 223–238.
- Srivastav, A. L., Singh, P. K., Srivastava, V., & Sharma, Y. C. (2013). Application of a new adsorbent for fluoride removal from aqueous solutions. *Journal of Hazardous Materials*, 263, 342–352.
- Tor, A. (2006). Removal of fluoride from an aqueous solution by using montmorillonite. *Desalination*, 2006(201), 267–276.
- Varaprasad, K., Nunez, D., Yallapu, M. M., Jayaramudu, T., Elgueta, E., & Oyarzun, P. (2018). Nano-hydroxyapatite polymeric hydrogels for dye removal. *RSC Advances*, 8, 18118–18127.
- Wang, X., Xu, H., & Wang, D. (2020). Mechanism of fluoride removal by $AlCl_3$ and AlI_3 : The role of aluminum speciation. *Journal of Hazardous Materials*, 398, 122987.
- Wang, Z., Zhao, Y., & Wen, T. (2022). Enhanced removal of fluoride from water through precise regulation of active aluminum phase using $CaCO_3$. *Environmental Science and Pollution Research*. <https://doi.org/10.1007/s11356-022-20641-z>
- WHO. (2006). Chemical fact sheets: Fluoride, third ed., Guidelines for Drinking Water Quality (Electronic Resource): Incorporation First Addendum. Recommendations, vol. 1, WHO, Geneva. 375–377.
- Wongrueng, A., Sookwong, B., Rakruam, P., & Wattanachira, S. (2016). Kinetic adsorption of fluoride from an aqueous solution onto a dolomite sorbent. *Eng. J.*, 20, 1–9.
- Yadav, K. K., Gupta, N., Kumar, V., Khan, S., & Kumar, A. (2018). A review of emerging adsorbents and current demand for defluoridation of water: Bright future in water sustainability. *Environment International*, 111, 80–108.
- Yami, T. L., Chamberlain, J. F., Butler, E. C., & Sabatini, D. A. (2016). Using a high-capacity chemically activated cow bone to remove fluoride: Field-scale column tests and laboratory regeneration studies. *Journal of Environmental Engineering*, 143, 04016083.
- Yilmaz, M., Al-Musawi, T. J., & Saloot, M. K. (2022). Synthesis of activated carbon from Lemna minor plant and magnetized with iron (III) oxide magnetic nanoparticles and its application in removal of Ciprofloxacin. *Biomass Conversion and Biorefinery*. <https://doi.org/10.1007/s13399-021-02279-y>
- Yu, X. L., Tong, S. R., Ge, M. F., & Zuo, J. C. (2013). Removal of fluoride from drinking water by cellulose-hydroxyapatite nanocomposites. *Carbohydrate Polymers*, 92, 269–275.
- Yu, C., Liu, L., & Wang, X. (2022). Fluoride removal performance of highly porous activated alumina. *Journal of Sol-Gel Science and Technology*. <https://doi.org/10.1007/s10971-022-05722-2>
- Zazouli, M. A., Balarak, D., Karimzadeh, F., & Khosravi, F. (2014a). Removal of fluoride from aqueous solution by using of adsorption onto modified Lemna minor: Adsorption isotherm and kinetics study. *Journal of Mazandaran University of Medical Sciences*, 23(109), 208–217.
- Zazouli, M. A., Mahvi, A. H., Dobaradaran, S., Barafshatehpour, M., & Mahdavi, Y. (2014b). Adsorption of fluoride from aqueous solution by modified Azolla Filiculoides. *Fluoride*, 47(4), 349–358.
- Zazouli, M. A., Mahvi, A. H., & Mahdavi, Y. (2015). Isothermic and kinetic modeling of fluoride removal from water by means of the natural biosorbents sorghum. *Fluoride*, 48(1), 15–22.
- Zhen, J., Yong, J., & Kai-Sheng, Z. (2016). Effective removal of fluoride by porous MgO nanoplates and its adsorption mechanism. *Journal of Alloys and Compounds*, 675, 292–300.
- Zhijie, Z., Yue, T. & Menggen, Z. (2011). Defluorination of wastewater by calcium chloride modified natural zeolite. *Desalination*, 276, 246–252.
- Zúñiga-Muro, N. M., Bonilla-Petriciolet, A., Mendoza-Castillo, D. I., & Reynel-Ávila, H. E. (2014). Fluoride adsorption properties of cerium-containing bone char. *Journal of Fluorine Chemistry*, 197, 63–73.

Publisher's Note Springer Nature remains neutral with regard to jurisdictional claims in published maps and institutional affiliations.

Springer Nature or its licensor holds exclusive rights to this article under a publishing agreement with the author(s) or other rightsholder(s); author self-archiving of the accepted manuscript version of this article is solely governed by the terms of such publishing agreement and applicable law.